

HELICAL BLOWOUT JETS IN THE SUN: UNTWISTING AND PROPAGATION OF WAVES.

E. J. LEE, V. ARCHONTIS AND A.W. HOOD

School of Mathematics and Statistics, University of St. Andrews, St. Andrews, KY169SS, UK

Draft version August 19, 2021

ABSTRACT

We report on numerical experiment of the recurrent onset of helical “blowout” jets in an emerging flux region (EFR). We find that these jets are running with velocities of $\sim 100 - 250$ km/s and they transfer a vast amount of heavy plasma into the outer solar atmosphere. During their emission, they undergo an untwisting motion as a result of reconnection between the twisted emerging and the non-twisted pre-existing magnetic field in the solar atmosphere. For the first time in the context of blowout jets, we provide a direct evidence that their untwisting motion is associated with the propagation of torsional Alfvén waves in the corona.

Subject headings: Sun: activity – Sun: interior – Sun: Magnetic fields –Magnetohydrodynamics (MHD) – methods: numerical

1. INTRODUCTION

Solar jets have been observed at various wavelengths (e.g. H α (Schmieder et al. 1995; Canfield et al. 1996), EUV and X-ray (Shibata et al. 1992; Alexander & Fletcher 1999)). They occur in EFR (e.g. Shibata et al. 1992), active regions (e.g. Canfield et al. 1996; Shimojo et al. 1996), coronal holes (e.g. Wang et al. 1998; Cirtain et al. 2007) etc. Recently a dichotomy of jets was suggested by Moore et al. (2010). About two thirds of the observed jets fit the “standard” reconnection picture, which invokes reconnection between oppositely directed magnetic fields, e.g. an emerging and a pre-existing magnetic field (e.g. Heyvaerts et al. 1977). The other one third have been termed “blowout” jets, which are triggered by an eruption. More precisely, it has been observed (e.g. Moore et al. 2010; Sterling et al. 2010; Shen et al. 2012) that the precursor of a “blowout” jet, is a twisted and/or a sheared arch, which often carries a (small) filament or flux rope within it. When this structure becomes unstable and erupts, it blows out the envelope field producing an untwisting ejection of cool (e.g. chromospheric) and hot material. This “blowout” jet is a broad, curtain-like structure in opposition to the “standard” jet, which is more elongated and it is not commonly associated with an eruption event.

Three-dimensional (3D) simulations on the formation of blowout jets, during the emergence and eruption of solar magnetic fields, have been carried out by Archontis & Hood (2013), Moreno-Insertis & Galsgaard (2013) & Fang et al. (2014). Archontis & Hood (2013) have shown that the interaction between an emerging (twisted) magnetic field and an ambient (non-twisted) magnetic field in the solar corona can trigger both standard and “blowout” jets. Their experiments reproduced some of the observed characteristics of the blowout jets, their internal helical structure and their overall curtain-like shape. Moreno-Insertis & Galsgaard (2013) studied the recurrent onset of eruptions in an EFR and their possible relationship to the subsequent emission of “blowout” jets. Using a similar numerical set-up, Fang et al. (2014) showed that heat conduction leads to an increase of the total mass ejection in the corona during the emission of the “blowout” jets. In previous simulations, Shibata & Uchida (1985) had shown that an unwinding jet could be the result of reconnection between a twisted loop and an open flux tube. The

unwinding motion, which has also been reported in observations (e.g. Cirtain et al. 2007; Moore et al. 2013) has been interpreted as the propagation of torsional Alfvén waves (see also Nishizuka et al. 2008) releasing the stored twist from a twisted magnetic loop into the open ambient field. However, no *direct* evidence of *propagating* Alfvén waves in “blowout” jets has been provided so far, either on numerical or observational studies.

Here, we report on the recurrent emission of “blowout” jets in an EFR with a sea-serpent configuration. We show that the “blowout” jets are untwisted during their ejection and, for the first time, we provide direct evidence of propagating torsional Alfvén waves during the emission of the “blowout” jets.

2. THE MODEL

We solve the 3D time-dependent, resistive and compressible MHD equations in Cartesian geometry, using the Lare3d code (Arber et al. 2001). Explicit (uniform) resistivity of $\eta = 10^{-2}$ is included.

The initial atmosphere consists of horizontal and homogeneous parallel layers in hydrostatic equilibrium. The solar interior is represented by a layer in the range $(-5.4 \text{ Mm} \leq z < 0 \text{ Mm})$, which is adiabatically stratified. The photosphere/chromosphere layer lies at $0 \text{ Mm} \leq z < 1.9 \text{ Mm}$. The temperature at the photosphere is 5100 K and it increases up to $\approx 3 \times 10^4 \text{ K}$ at the top chromosphere. The transition region is located at heights $1.9 \text{ Mm} \leq z \leq 2.7 \text{ Mm}$. Above it, there is an isothermal layer ($\mathcal{O}(1) \text{ MK}$), which is mimicking the lower solar corona ($2.7 \text{ Mm} < z \leq 57.6 \text{ Mm}$). In the solar interior, the magnetic field is a horizontal magnetic flux tube, which is twisted. The flux tube is located at $z_0 = -2.1 \text{ Mm}$ and its axis is parallel to the y-axis at $x = 0$. The component of the magnetic field along the tube’s axis (axial field) is given by

$$B_y = B_0 \exp(-r^2/R^2), \quad B_\theta = \alpha r B_y, \quad (1)$$

where the tube’s radius is $R = 450 \text{ km}$ and r is the radial distance from the tube’s axis ($r^2 = x^2 + (z - z_0)^2$). The twist of the fieldlines around the tube’s axis is uniform and it is given by $\alpha = 2.2 \times 10^{-3} \text{ km}^{-1}$. With this twist the tube is marginally stable to the kink instability. Initially, we apply a deficit in density along the tube’s axis, making two segments (i.e. at $x = 0$, $y = \pm 3.2 \text{ Mm}$) more buoyant than the rest of

the tube:

$$\Delta\rho = [p_t(r)/p(z)]\rho(z)\exp(-y^2/\lambda^2)\sin^2(2\pi y/\omega). \quad (2)$$

Thus, $\Delta\rho$ is the difference between the background density and the density inside the flux tube after we apply the density deficit along its axis. The pressure within the flux tube is p_t , λ defines half the length of each buoyant part of the tube, and ω is defined as half of the flux tube length. We use $\lambda = 3.6$ Mm, $\omega = 31.5$ Mm and an initial field strength of $B_0 = 2.4$ kG, which corresponds to plasma $\beta \approx 28$. The corona is filled with an ambient field which is oblique, and is defined by

$$B_c = B_c(z)(0, \cos\theta, \sin\theta), \quad (3)$$

where $\theta = 80^\circ$, and $B_c(z) \approx 3$ G for $z \geq 0.54$ Mm, and gradually decreases to 0 for $z < 0.54$ Mm. The numerical domain is $[-31.5, 31.5] \times [-31.5, 31.5] \times [-5.4, 57.6]$ Mm in the direction perpendicular to the tube (x), along the tube's axis (y) and vertical (z), respectively. The numerical grid is a 420^3 box with periodic boundary conditions in x and y direction. At the top, there is an open boundary allowing plasma to flow out of the grid. There is a non-penetrating, conducting wall at the bottom boundary.

3. RESULTS AND DISCUSSION

In the following, we discuss the results of our simulations showing: (a) the emergence of the sea-serpent flux tube at the photosphere, (b) the recurrent onset of the jets and (c) the propagation of torsional Alfvén waves during the untwisting motion of the blowout jet(s). Figure 1(a) shows the initial (i.e. at $t = 0$) topology of the magnetic field. Figure 1(b) shows the connectivity of the fieldlines during the first blowout jet emission. The (blue) fieldlines show (a) the sea-serpent configuration of the emerging field and (b) the twisted fieldlines at the center of the EFR, which are the result of reconnection between the emerging loops. The (red) fieldlines are reconnected fieldlines that join the ambient with the emerging field. Due to the sea-serpent configuration, the downward tension of the uppermost fieldlines (i.e. the envelope field) of each emerging loop is released more effectively due to reconnection with (*both*) the ambient field and the field of the neighbouring emerging loop. Thus, unavoidably, this interaction affects the onset time and dynamics of the EFR's eruptions, compared to a "single emerging loop - ambient field" reconnection case (e.g. Archontis & Hood 2013).

Figure 2(a) shows the magnetogram during the emergence of the field into the photosphere at $t \simeq 165.7$ min. The overplotted arrows represent the direction of the magnetic field vector. Due to the initial density deficit, the emerging magnetic field at the solar surface forms two bipolar regions (hereafter, BR1 and BR2). At $t \simeq 237.1$ min (Figure 2(b)), the polarities of each BR have moved apart along the y -direction. In previous studies (e.g. Archontis & Török 2008), it has been shown that this movement is followed by shearing along the polarity inversion line (PIL), and the formation of a new flux rope, which might erupt into the corona. This is also found to happen in the present simulation, within each BR. Moreover, we find that shearing and reconnection leading to the formation of a flux rope, occurs also between the opposite polarities P1 and N2 due to their relative motion.

Before the onset of the eruptions ($t < 200$ min), each emerging bipole comes into contact and eventually reconnects with the ambient magnetic field, giving onset to hot reconnection jets. Figures 2(c) and 2(d) show the temperature and v_z

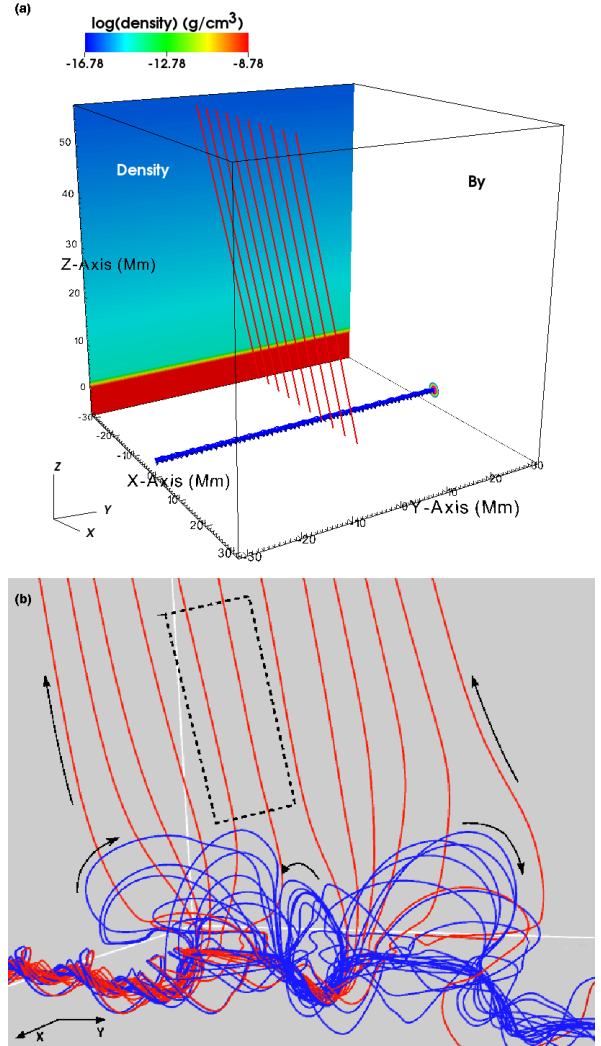


FIG. 1.— (a) Selected magnetic fieldlines (red) show the orientation of the oblique magnetic field in the corona. The twisted magnetic flux tube is shown by the blue fieldlines. The coloured, vertical y - z plane shows the density distribution of the background atmosphere. Isocontours at the x - z plane represent B_y . (b) A close-up of the fieldline topology ($t = 232.8$ min). Fieldlines have been traced from the two emerging bipoles (blue) and from the ambient field (red). Arrows show the direction of the magnetic field. The (dashed) rectangle indicates the channel along which the first blowout jet is emitted.

distribution respectively, at $x = 0$ and $t \simeq 165.7$ min. We find that the upward reconnection jets are moving with a velocity of ~ 40 km/s, reaching temperatures of up to 1×10^6 K at the reconnection site, and 8×10^5 K within the jet channels.

Figures 2(e) and 2(f) show the first eruptive event within the EFR. The eruption of the cool plasma starts within BR2. Figure 2(e) shows the temperature and figure 2(f) shows the density distribution at $y \simeq -2$ Mm and $t = 230$ min. The rise of the erupting material induces inflow towards the interface, where a current layer has built up, between the envelope and the ambient field. This leads to more external reconnection between the two magnetic flux systems and the onset of a hot and fast external reconnection jet. The plasma at the interface is heated up to 3.5×10^6 K. A side-effect of the external reconnection is the formation of a hot external arcade with temperature up to 5.5×10^6 K.

At $t \simeq 232.8$ min (Figures 2(g), 2(h)), the eruption blows out the envelope field and the dense erupting material is emit-

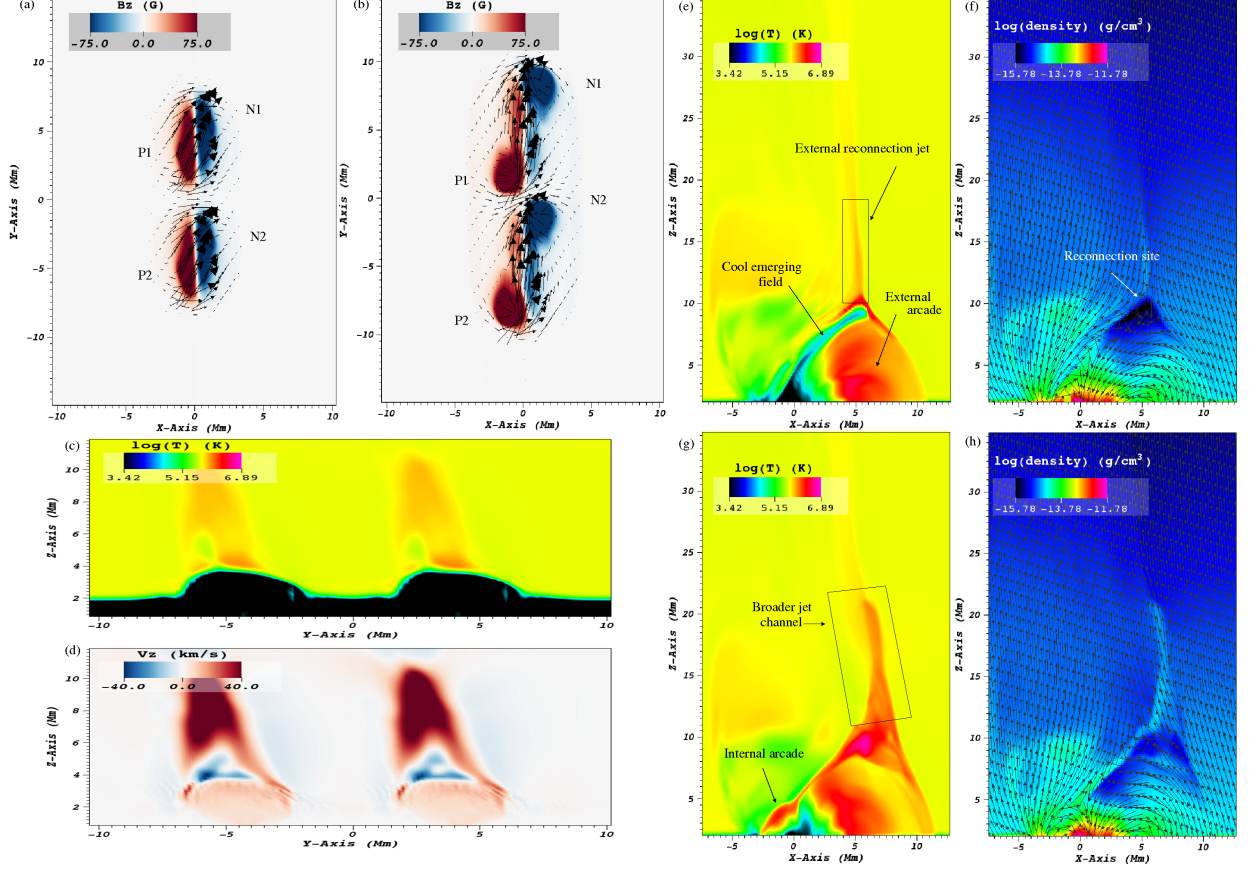


FIG. 2.— The magnetogram during the emergence at the photosphere, showing the two bipolar regions (BR1 consisting of N1,P1 and BR2 consisting of N2,P2) at two times: (a) $t = 165.7$ min and (b) $t = 237.1$ min. Temperature (c) and v_z (d) distribution during the emission of the reconnection jets at $t = 165.7$ min at $x = 0$ Mm. Temperature (e) and density (f) distribution during the eruption preceding the first blowout jet at $t = 230.0$ min. Temperature (g) and density (h) distribution during the first "blowout" jet at $t = 232.8$ min. Arrows denote the direction of the magnetic field vector (projected onto the plane). The vertical slice in (e-h) is at $y = -2$ Mm.

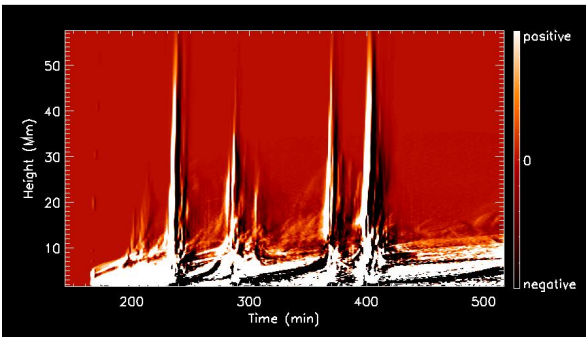
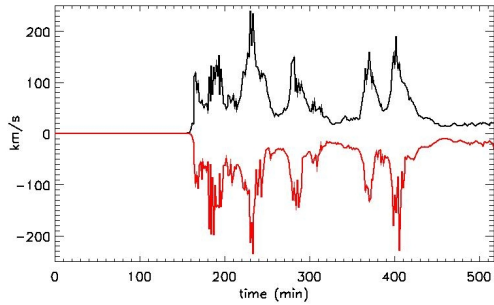


FIG. 3.— **Top:** Temporal evolution of the maximum (black) & minimum (red) v_z above the photosphere. **Bottom:** Height-time diagram (running difference) of $\int \rho^2 dx dy$, where $T > 8 \times 10^5$ K.

ted along the reconnected fieldlines of the oblique ambient

field. Now the channel of the blowout jet and the external arcade are much wider. Cool (5×10^5 K) and hot (1×10^6 K) plasmas are ejected along the blowout jet's channel and heating (due to internal reconnection) is produced underneath the erupting plasma, where an internal arcade of temperature up to 4×10^6 K is formed.

The top panel in Figure 3 shows that there are six events during which v_z varies in the range $\sim 100 - 250$ km/s. Each event consists of several peaks in v_z . The fact that the peaks of minimum and maximum v_z occur at approximately the same time suggests the existence of bidirectional flows from several sites within the EFR. We find that the first peak ($t \approx 165$ min) corresponds to the jets caused by reconnection between the emerging and the ambient magnetic field. The second event ($t \approx 185 - 210$ min, $v_z \sim 150$ km/s) is the composite effect of an eruption, which starts from the area in between BR1 and BR2, and a reconnection jet that follows the eruption. The jet is initiated due to the restructuring of the nearby magnetic field due to the eruption (in a similar manner to the external reconnection jet in Figure 2e). However, in this occasion, the erupting plasma becomes confined by the local ambient field and does not evolve into a profound blowout jet that could reach the higher solar atmosphere. Instead, it is moving sideways, from the center of the EFR towards the BR1 where the total pressure is less.

The other four events correspond to the emission of "blowout" jets driven by eruptions that emanate from within the BRs. These jets blast heavy material towards the outer

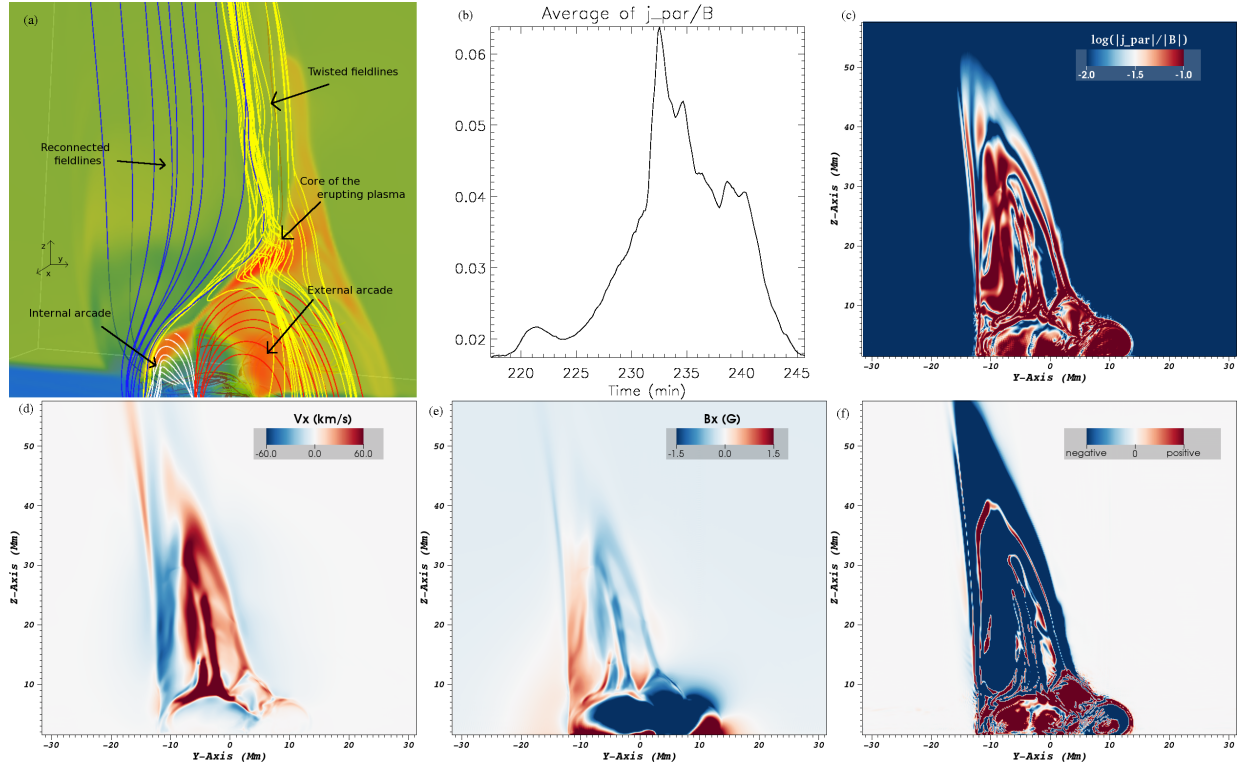


FIG. 4.— (a) Visualization of the magnetic fieldlines, showing the helical nature of the blowout jet (yellow), the reconnected fieldlines that join the emerging with the ambient field (blue), the internal arcade (white) and the external arcade (red). (b) The temporal evolution of the average $j_{\parallel}/|B|$ within the blowout jet. (c): The $|j_{\parallel}|/|B|$ distribution, (d): v_x distribution, and (e): B_x distribution, at $x = 5.4$ Mm, $t = 233.4$ min. (f): $j_{\parallel} \cdot \omega_{\parallel}$, where j_{\parallel} (ω_{\parallel}) is the current (vorticity) parallel to the reconnected fieldlines.

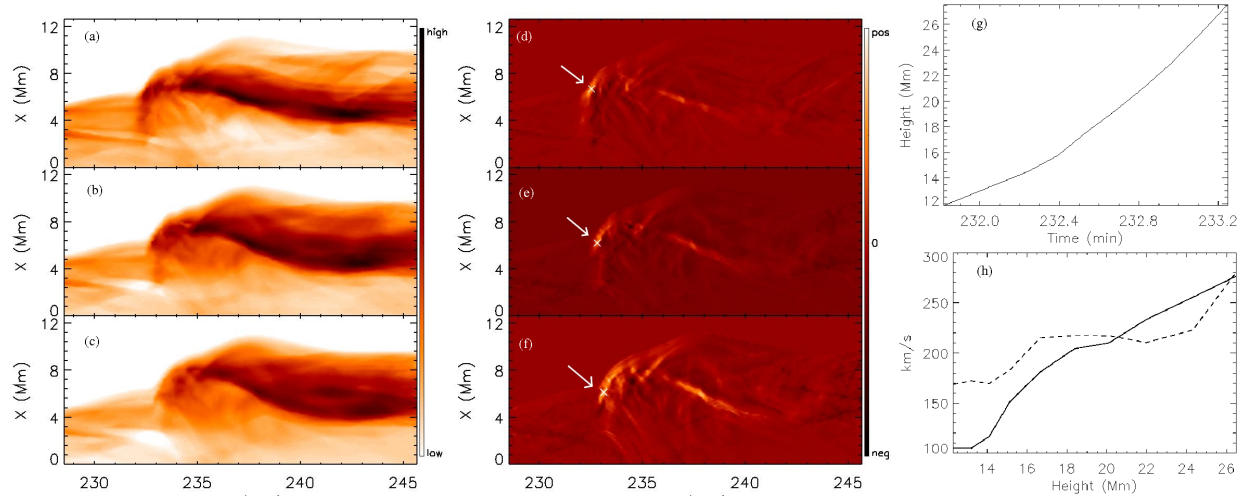


FIG. 5.— The distance-time diagram of $\int \rho^2 dy$, for $0.6 \text{ mK} < T < 1.2 \text{ mK}$, across the jet at (a) 17 Mm, (b) 21.5 Mm and (c) 25 Mm. (d,e,f) are the running difference of (a,b,c) respectively. (g) shows the height-time profile of the heavy front of the jet, obtained by tracing the first maximum of the running difference (white cross in (d,e,f)) at various heights. The velocity of this front is shown in panel (h). The dashed line in (h) is the local Alfvén speed in the close vicinity of the front of the wave.

solar atmosphere. The bottom panel in Figure 3 shows the running difference of the integrated plasma density $I = \int \rho^2 dx dy$ for temperatures above $8 \times 10^5 \text{ K}$. It is found that there are four marked events during which dense plasma is brought into the higher atmosphere. The steep vertical slope at the end of each event indicates that most of the ejected plasma is transported upwards. The dark regions after the brightening peaks indicate that part of the erupting plasma undergoes gravitational draining. Notice that the time-period between the onset of the blowout jets is not so “quiet”. There

are various, less striking events, which do not dump enough mass and energy into the outer corona. Such events (e.g. at $t \approx 190 - 210 \text{ min}$, $t \approx 310 \text{ min}$, etc.) are small confined eruptions and reconnection coronal jets. By comparing the two panels in Figure 3, we find a good temporal correlation between the four “blowout” jets and the emission of bidirectional flows, which occur after $t \approx 220 \text{ min}$. This is a direct evidence that the “blowout” jets are closely associated with reconnection, which is driven by the eruption of cool material from the low atmosphere.

The erupting core of the blowout jets is a twisted flux tube. Figure 4(a) illustrates the magnetic fieldlines within and around the first blowout jet (see also Archontis & Hood 2013). Reconnection of the erupting (twisted) field with the open (non-twisted) ambient field would most likely relax the twist and lead to an untwisting motion of the helical blowout jet. A measurement of the twist is given by j_{\parallel}/B , where j_{\parallel} is the parallel component of the current along the reconnected fieldlines of the blowout jet. Figure 4(b) shows the temporal evolution of the average $|j_{\parallel}|/B$ along the channel of the blowout jet. We calculate this for heights above $z \approx 9$ Mm, which is the approximate horizontal boundary between the envelope field of the emerging flux and the lower part of the blowout jet. The increase of the twist (up to $t = 235$ min) is due to the eruption of the flux rope and the subsequent decrease indicates the untwisting motion of the jet. Figure 4(c) shows the distribution of $|j_{\parallel}|/B$ at the vertical slice with $x = 5.4$ Mm. It is confirmed that the blowout jet possess considerable twist along its main stream (e.g. in the range $z = 10-40$ Mm). Notice that $|j_{\parallel}|/B$ is also very strong (as expected) in the twisted emerging field underneath the blowout jet (e.g. the area with strong B_x at $z < 7$ Mm).

To show the untwisting motion of the jet, we plot the v_x and B_x distribution (Figures 4(d) and 4(e) respectively). There is positive v_x (pointing out of the plane) at the right-hand side of the jet, and negative v_x (pointing into the plane) at the left-hand side. This corresponds to a magnetized plasma motion where B_x (i.e. the transverse component of the magnetic field) is pointing in the opposite direction to v_x and the associated vorticity (i.e. $\vec{\omega} = \nabla \times \vec{v}$) is pointing downward. This is a first indication that the jet undergoes an untwisting motion. More evidence is found by studying the distribution of current and vorticity within the jet.

Figure 4(f) shows the product of j_{\parallel} with the vorticity ω_{\parallel} . Within the jet channel, this product is mostly negative indicating that the current and vorticity are pointing in different directions. In fact, we have found (not shown in this figure) that ω_{\parallel} is negative due to the direction of the flow (and it is pointing downwards), while j_{\parallel} is positive due to the direction of the twist of the fieldlines (pointing upwards). All the above support the scenario of the untwisting motion of the blowout jet during its emission. It is likely that the process of untwisting of the erupting plasma in our experiment is similar to the sweeping-magnetic-twist mechanism for the acceleration of solar jets (Shibata & Uchida 1985). In the present simulation, it is apparent that the twist stored in the erupting flux is released along the direction of the open, reconnected field lines. Also, the direction of the untwisting motion (e.g. as shown in Figure 4) is consistent with the relative orientation of the two field components (i.e. the erupting and the open field) that reconnect. Thus, it is more likely that the untwisting is related to the propagation of the twist along the reconnected fieldlines instead of the twist itself.

To study the plasma motion of the jet, in relation to the

direction of the ambient field, we calculate $I_1 = \int \rho^2 dy$ at various heights, from $z \approx 12$ Mm to $z \approx 27.5$ Mm. More precisely, we take a horizontal slit at each height and we plot the above quantity, I_1 , during the evolution of the system. The left panel in Figure 5 shows I_1 at $z = 17$ Mm, $z = 21.5$ Mm and $z = 25$ Mm. We trace plasma of temperature between 6×10^5 K and 1.2×10^6 K. We find that firstly the plasma jet is moving towards the positive x direction, then to the negative x direction, and then back towards the positive x direction. This indicates that the jet undergoes an oscillatory motion during its emission. A similar result, in the context of helical jets, has been reported by Liu et al. (2009). The transverse oscillation velocity amplitude of the jet is $\approx 7 \text{ km s}^{-1}$. Figure 5 (a-c) shows that the oscillation propagates from low to larger heights. Since the jet is considered to be emitted along the ambient magnetic field, this is an evidence of a wave propagating towards the outer solar atmosphere.

To measure the velocity of the propagating wave, we use the height-time diagrams in panels (a)-(c) and we plot the running-difference of each panel, as shown in panels (d)-(f). Then, we find the first (i.e. along time) local maximum in each running-difference plot, which corresponds to the first profound increment of plasma density at that height. It is likely that this point is located at the front of the heavy plasma distribution along the jet. The height-time profile of this front is then plotted in Figure 5(g) and by calculating the gradient, we obtain the propagating speed (Figure 5(h)). The latter is comparable to the local Alfvén speed, which suggests that we are witnessing the propagation of a torsional Alfvén wave during the untwisting motion of the blowout jet. We find that the above result is generic: all the blowout jets in our experiment show transverse oscillatory motions and encompass propagating Alfvén waves along their broad outflow streams.

3.1. Discussion

The initial ambient open field in our experiment has a field strength of approximately 3 G. The density in the high corona is approximately $10^{-16} \text{ g cm}^{-3}$. Therefore, our simulation is mimicking the emission of jets in a coronal hole environment. We have calculated that in every blowout jet emission, a considerable amount of Poynting energy flux ($\mathcal{O}(10^5) \text{ erg s}^{-1} \text{ cm}^{-2}$) leaves the high corona. Also the mass deposition in the corona increases by a factor of 2-4 during the blowout ejecta. It is likely that the torsional Alfvén waves transport the emitted flux from the low corona to the outer atmosphere and load with mass the open field. This implies that blowout jets may play a significant role in driving the solar wind.

The simulations were performed on the STFC and SRIF funded UKMHD cluster, at the University of St Andrews. VA acknowledges support by the Royal Society. We would like to thank the anonymous Referee for comments and suggestions on how to improve the manuscript.

REFERENCES

- Alexander, D., & Fletcher, L. 1999, *Sol. Phys.*, 190, 167
 Arber, T., Longbottom, A., Gerrard, C., & Milne, A. 2001, *Journal of Comp. Phys.*, 171, 151
 Archontis, V., & Hood, A. W. 2013, *ApJ*, 769, L21
 Archontis, V., & Török, T. 2008, *A&A*, 492, L35
 Canfield, R. C., Peardon, K. P., Leka, K. D., Shibata, K., Yokoyama, T., & Shimojo, M. 1996, *ApJ*, 464, 1016
 Cirtain, J. W., et al. 2007, *Science*, 318, 1580
 Fang, F., Fan, Y. & McIntosh, S. W. 2014, *ApJ*, 789, L19
 Heyvaerts, J., Priest, E. R., & Rust, D. M. 1977, *ApJ*, 216, 123
 Liu, W.L., Berger, T. E., Title, A. M., & Tarbell, T. D 2009, *ApJ*, 707, L37
 Moore, R. L., Cirtain, J. W., Sterling, A. C., & Falconer, D. A 2010, *ApJ*, 720, 757
 Moore, R. L., Sterling, A. C., Falconer, D. A., & Robe, D. 2010, *ApJ*, 769, 134
 Moreno-Inertis, F., & Galsgaard, K. 2013, *ApJ*, 771, 20

- Nishizuka, N., Shimizu, M., Nakamura, T., Otsuji, K., Okamoto, T. J., Katsukawa, Y., & Shibata, K. 2008, *ApJ*, 683, L83
- Schmieder, B., Shibata, K., van Driel-Gesztelyi, L., & Freeland, S. 1995, *Sol. Phys.*, 156, 245
- Shibata, K., & Uchida, Y. 1985, *PASJ*, 37, 31
- Shibata, K., et al. 1992, *PASJ*, 44, L173
- Shimojo, M., et al. 1992, *PASJ*, 48, 123
- Shen, Y., Liu, Y., Su, J., & Deng, Y. 2012, *ApJ*, 745, 164
- Sterling, A. C., Harra, L. K. & Moore, R. L. 2010, *ApJ*, 722, 1644
- Wang, Y.-M., et al. 1998, *ApJ*, 508, 899